Friction, slip and structural inhomogeneity of the buried interface

2011 Modelling Simul. Mater. Sci. Eng. 19 065003

(http://iopscience.iop.org/0965-0393/19/6/065003)

Modelling Simul. Mater. Sci. Eng. **19** (2011) 065003 (15pp) doi:10.1088/0965-0393/19/6/065003

Friction, slip and structural inhomogeneity of the buried interface

Y Dong[1], Q Li[2], J Wu[1] and A Martini[1]

[1] Purdue University, West Lafayette, IN 47907, USA
[2] University of Pennsylvania, Philadelphia, PA 19104, USA

E-mail: a-martini@purdue.edu

Received 18 November 2010, in final form 26 April 2011
Published 15 July 2011
Online at stacks.iop.org/MSMSE/19/065003

Abstract

An atomistic model of metallic contacts using realistic interatomic potentials is used to study the connection between friction, slip and the structure of the buried interface. Incommensurability induced by misalignment and lattice mismatch is modeled with contact sizes that are large enough to observe superstructures formed by the relative orientations of the surfaces. The periodicity of the superstructures is quantitatively related to inhomogeneous shear stress distributions in the contact area, and a reduced order model is used to clarify the connection between friction and structural inhomogeneity. Finally, the movement of atoms is evaluated before, during and after slip in both aligned and misaligned contacts to understand how the interfacial structure affects the mechanisms of slip and the corresponding frictional behavior.

(Some figures in this article are in colour only in the electronic version)

1. Introduction

Atomic-scale friction arising from single-asperity contact has been widely studied as a means of gaining insight into the fundamental mechanisms by which friction occurs. Experimentally, these studies are often performed using an atomic force microscope (AFM) where a nano-scale sharp tip approximating a single asperity is scanned laterally across a substrate and the resulting friction forces are measured. These measurements have shed light on many characteristics of atomic-scale friction and their material and condition dependences. Further, recent experimental findings have shown that details in the buried interface may play a critical role in understanding these measurements [1].

An important characteristic of the buried interface in determining friction, and the one we focus on here, is commensurability. Increasing numbers of AFM measurements have shown that incommensurability can lead to very low friction (see for example [2–4]), an effect that has been called 'structural lubricity' [5]. Particulary relevant to this work are measurements

0965-0393/11/065003+15$33.00

of a graphite flake sliding on graphite at different orientations where very low friction was achieved *except* when the relative rotation angle of the graphite surfaces was a multiple of 60°, a value that coincides with the symmetry of graphite lattice [4]. These findings clearly illustrate that there is a connection between commensurability and friction.

To fully understand the mechanisms underlying these observations requires availability of information about the interface between the tip and substrate. Unfortunately, so far it has been extremely difficult to directly observe the atomic-scale phenomena within a buried interface during sliding using experimental methods. Therefore, experiments are often complemented by models of AFM tip and substrate interactions. Specifically, reduced-order models (see for example [6–8]) and fully atomistic molecular dynamics (MD) simulations (see for example [8–10]) have been used to gain insight into how incommensurability enables ultra-low friction.

In this study we significantly extend previous work by applying a fully atomistic model of metallic contact using realistic interatomic potentials and a complementary multi-atom 1D Frenkel–Kontorova–Tomlinson (FKT) model. The goal of the research is to understand the connection between friction and the atomic structure of the buried interface. We study the effects of misalignment using contact sizes that are large enough to observe superlattices formed by the relative orientations of the surfaces, and the periodicity of the superlattices is quantitatively related to inhomogeneous shear stress distributions in the contact area. Then, the 1D FKT model is used to understand these relationships. Finally, we analyze the atomic displacement and shear stress distributions during slip to understand how relative motion occurs in aligned and misaligned contacts.

2. Methodology

2.1. Molecular dynamics simulation

The atomistic model consists of a platinum tip and a gold substrate as illustrated by the snapshots in figure 1. These materials are selected because of the similarity of their lattice constants ($a_{Au} = 0.408$ nm and $a_{Pt} = 0.392$ nm) which enables study of misalignment-induced incommensurability while minimizing the welding that is sometimes observed in sliding contact between two surfaces of the same material. The geometry of the model is similar to one we have reported before [11] where the tip is a truncated cone. In this case, the radii of the cone at the top and bottom (i.e. contact area) are 2.2 nm and 1.4 nm, respectively. The substrate is 2.12 nm thick (nine atomic layers in the z-direction), 5.77 nm long (x-direction) and 5.00 nm wide (y-direction) and periodic boundary conditions are applied in the x- and y-directions. The contact occurs at the face centered cubic (fcc) {1 1 1} surface which has the lowest surface energy and therefore discourages welding. We also briefly discuss a copper–silver system with the same simulation setup as the Pt/Au model except the contact radius is increased to 2 nm. All atomic interactions are modeled using the embedded atom method; details are given in the appendix.

The bottom three layers of the substrate and the top three layers of the tip are treated as rigid bodies. The rigid atoms of the tip are translated laterally along the [1 1 0] direction at a constant speed of 1 m s^{-1} and given freedom to move in the normal direction. A Langevin thermostat excluding the contribution of the imposed speed with a damping parameter on the order of 5 (ps)$^{-1}$ is applied to the atoms at least three layers away from the tip–substrate interface while the atoms near the interface are allowed to evolve according to Newtonian dynamics. Normal load is applied to the uppermost atomic layers of the tip. Recent experimental and computational studies have shown that, at low loads, friction varies little with load, while at high loads, significant cold welding can occur and stable stick–slip disappears [11, 12]. In order to

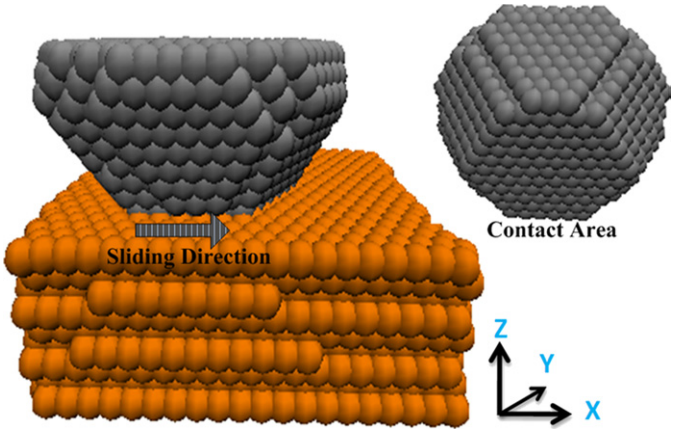

Figure 1. Snapshot of the MD simulation model of an AFM tip–substrate system; a bottom view of the tip is shown to the right illustrating the contact area.

achieve metal/metal sliding without cold welding or material transfer, we deliberately choose a relatively low external load (0 nN). Simulations are performed at 1 and 300 K and similar results are obtained at both temperatures. However, the figures shown in this paper correspond to 1 K (which exhibits less thermal noise) to facilitate understanding of the sometime subtle atomic details. Simulations are carried out using the LAMMPS [13] molecular dynamics software.

2.2. FKT model

The one-dimensional Frenkel–Kontorova–Tomlinson model [6–8, 14] is applied to help better understand the friction mechanisms. This model captures the interaction between tip and substrate as well as the coupling between tip atoms. An illustration of the FKT model is shown in figure 2 where a deformable chain of atoms is used to model the tip, and the total potential energy of the system can described as

$$V_{\mathrm{FKT}}(x,t) = \sum_{i=1}^{N} U\cos\left(\frac{2\pi x_i}{a}\right) + \sum_{i=1}^{N}\frac{k_1}{2}(vt + (i-1)b - x_i)^2 + \sum_{i=1}^{N-1}\frac{k_2}{2}(\Delta x_{i,i+1} - b)^2 \tag{1}$$

where N is the number of atoms, U is the amplitude of the sinusoidal corrugation potential, x_i is the displacement of the ith atom, a and b are respective substrate and tip lattice parameters, $\Delta x_{i,i+1}$ is the distance between atom i and adjacent atom $i+1$, v is the sliding speed of the support and t is the time. This expression includes the corrugation potential (the first term of of equation (1)), the elastic potential due to tethering to the support introduced by springs k_1 (second term), and the potential resulting from the interaction between tip atoms via elastic springs k_2 (third term).

By neglecting the thermal activation of the tip, the dynamics of each atom can be described by the Langevin equation,

$$m\ddot{x}_i + m\mu\dot{x}_i = -\frac{\partial V_{\mathrm{FKT}}}{\partial x_i}, \tag{2}$$

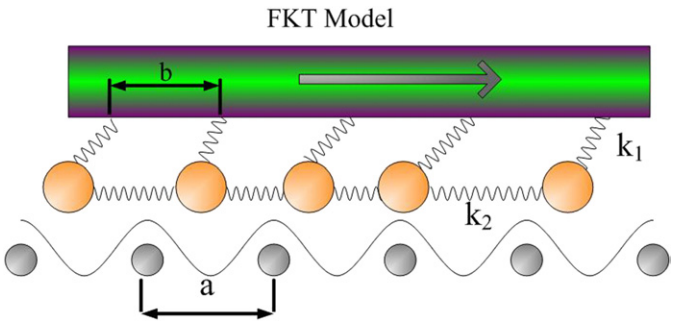

Figure 2. Illustration of the 1D Frenkel–Kontorova–Tomlinson model with $N = 5$ tip atoms.

where m is the tip mass and μ is the frictional damping coefficient describing the rate of energy dissipation. The friction force is then calculated by equation (3),

$$F = \sum_{i=1}^{N} k_1[vt + (i-1)b - x_i]. \tag{3}$$

For application to the Pt/Au system and to be consistent with values proposed by other researchers [7, 15], the model parameters are set as follows: $a = 0.288\,\text{nm}$, $m = 10^{-12}\,\text{kg}$, $U = 0.2\,\text{eV}$, $v = 0.2\,\mu\,\text{m}\,\text{s}^{-1}$ and μ is the critical damping $2\sqrt{k/m}$. The value of k_2 is selected to correlate with Pt metallic bonds. The typical stiffness of metallic bonds is in the range 15–75 $\text{N}\,\text{m}^{-1}$ [16]; we choose $k_2 = 50\,\text{N}\,\text{m}^{-1}$, which is reasonable for Pt. Determining an appropriate value for k_1 is not as straightforward since this parameter plays two distinct roles in the FKT model. The first is to model the overall stiffness of the tip and cantilever. Conventionally, k_1 is taken to be around 1–10 $\text{N}\,\text{m}^{-1}$ to capture the effective system stiffness [11, 17, 18]. However, k_1 should also describe the interaction between the atoms in the contact area and the rest of the tip, which suggests its magnitude should be consistent with metallic bonds. Considering these two effects, a value of $k_1 = 5\,\text{N}\,\text{m}^{-1}$ is used in this paper.

3. Results and discussion

3.1. Interface structure and shear stress

We investigate the effect of alignment by rotating the Pt tip relative to the Au substrate. Figure 3 shows the calculated maximum friction (the peak function or the instantaneous friction before slip) as a function of relative rotation angle. When the crystallographic orientations of the tip and substrate are aligned (i.e. $n \times 60^\circ$ where n is an integer), very high friction is observed. This is consistent with the behavior expected from commensurate contact and we therefore infer that the similarity of the Au and Pt lattice constants enables them to behave as quasi-commensurate when they are aligned. For simplicity, we will refer to the quasi-commensurate state as aligned contact for the rest of this paper. When the surfaces are rotated relative to each other, the friction drops a few orders of magnitude. This behavior is characteristic of incommensurate surfaces. The simulation results agree well with the experimental measurements of friction between graphite layers discussed in the introduction [4] which is not surprising since the {1 1 1} surface of the face-centered-cubic materials in our simulation exhibit a hexagonal pattern geometrically similar to that of graphite, i.e. both lattice structures are six-fold symmetric. Similar frictional behavior in aligned contact has been observed in other model systems [19, 21]. We also find that when the tip is rotated a small amount from perfect alignment, the rigid atoms at the top

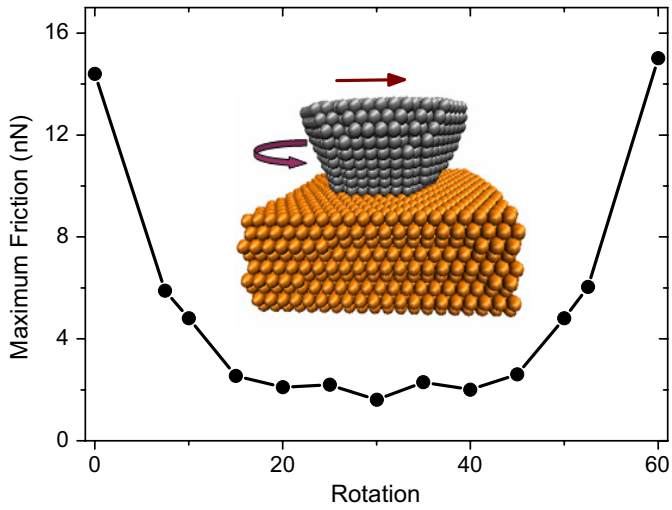

Figure 3. Maximum friction force as a function of relative tip–substrate orientation. A snapshot of the model is shown as an inset.

of the tip exert a strong torque that tends to force the lower layers of the tip to return to the aligned position which is consistent with another experimental observation of graphite [20].

To further investigate the significant frictional variation between aligned and misaligned configurations shown in figure 3, we evaluate the virial atomic shear stress at the buried interface. The virial atomic stress is defined to account for the effects of momentum change of both mechanical forces and mass transport. Although it is not equivalent to mechanical Cauchy stress [22], its distribution still provides a useful qualitative description of the stress variation along the interface. The virial stress reported here has units of pressure $\times$ volume (bar $\times$ Å^3) where the volume is that of an individual atom. The virial shear stress distributions before sliding at three different tip–substrate orientations are illustrated in figure 4. The stress distribution corresponding to the aligned system with a relative rotation of 0° (figure 4(*a*)) is homogeneous. However, for misaligned systems, such as those shown in figures 4(*b*) and (*c*) with relative rotations of 15° or 30°, the shear stress distribution in the contact area is divided into multiple subregions where the magnitude of the stress alternates between positive and negative.

It can also be seen from the upper images of figures 4(*b*) and (*c*) that the misalignment causes some lattice positions of the tip to coincide exactly with some lattice positions of the substrate. This overlap leads to the development of a superstructure or Moiré pattern. Indeed, there is quantitative prediction for periodicity of the Moiré pattern at a given misalignment angle for two contacts with identical structures [23, 24],

$$P_{\mathrm{M}} = \frac{L}{2\sin(\theta/2)}, \tag{4}$$

where L is the nearest atomic distance on the fcc {1 1 1} plane and θ is the misalignment angle. This formula is applicable to squared lattice and six-fold symmetric structures. For both Au and Pt, $L \approx 0.288$ nm, with which we can calculate the periodicity of the Moiré pattern for any angle. For example, at $\theta = 15°$, the periodicity of the Moiré pattern calculated using equation (4) is $P_{\mathrm{M}} = 1.1$ nm. We determine the periodicity of the shear stress distribution by measuring the distance between subregions with similar stress in figure 4(*b*) and find that its periodicity at $\theta = 15°$ is also ~1.1 nm, the same as that of the Morié pattern.

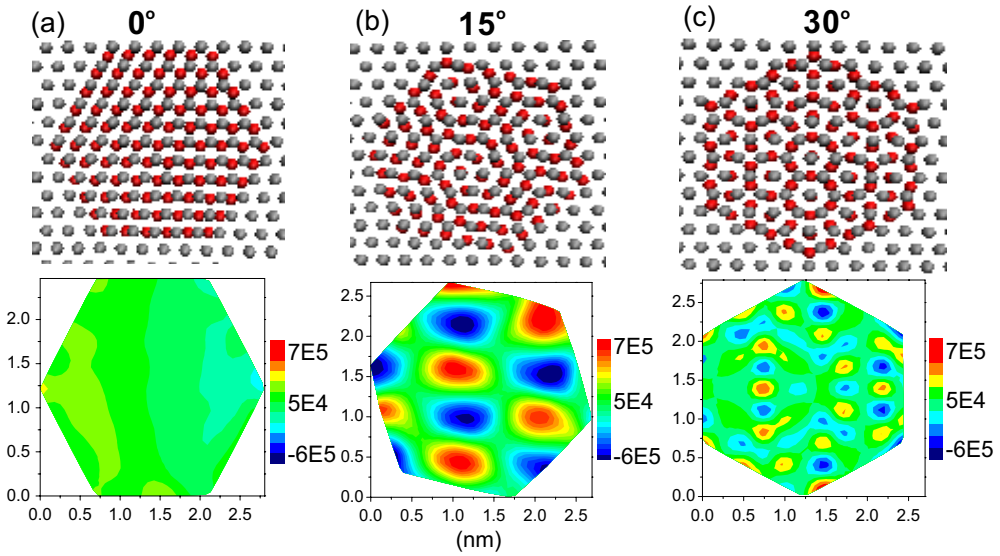

Figure 4. Moiré patterns (top) where the silver dots are substrate atoms and the red dots are tip atoms and the corresponding shear stress distribution (bottom) in the sliding direction for the Pt/Au system at relative rotations of (*a*) 0°, (*b*) 15° and (*c*) 30°.

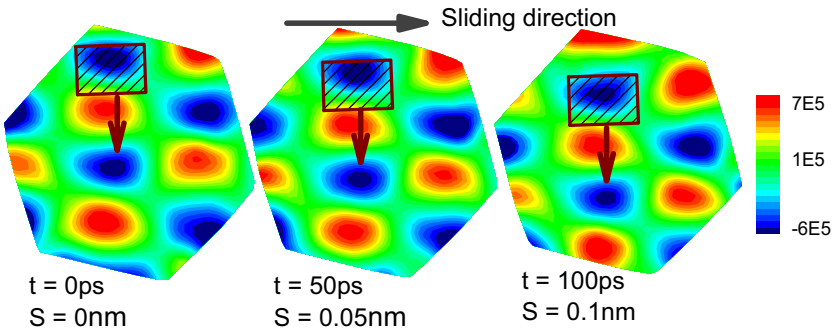

Figure 5. Propagation of the inhomogeneous stress distribution characteristic of incommensurate contact. The snapshots are taken at different times and sliding distances ($t = 0$ ps and $S = 0$ nm, $t = 50$ ps and $S = 0.05$ nm, $t = 100$ ps and $S = 0.1$ nm) from a system at $\theta = 15°$ relative rotation.

We also observe that, as the tip moves, the shear stress distributions evolve correspondingly. Figure 5 illustrates the evolution of the stress distribution at a rotation angle of $\theta = 15°$. The direction that the stress patterns move can be seen by tracking the position of one of the stress subregions. From figure 5 we can see that the highlighted stress subregion moves in a direction perpendicular to the direction the tip is sliding. The trends of consistency between superstructures and shear stress, and evolution of the shear stress distributions are observed at all misaligned orientations.

These results illustrate a clear relationship between atomic structure and shear stress in the contact area. One consequence of an inhomogeneous shear stress distribution is that the positive and negative forces in the interface counteract each other and lead to an overall lower

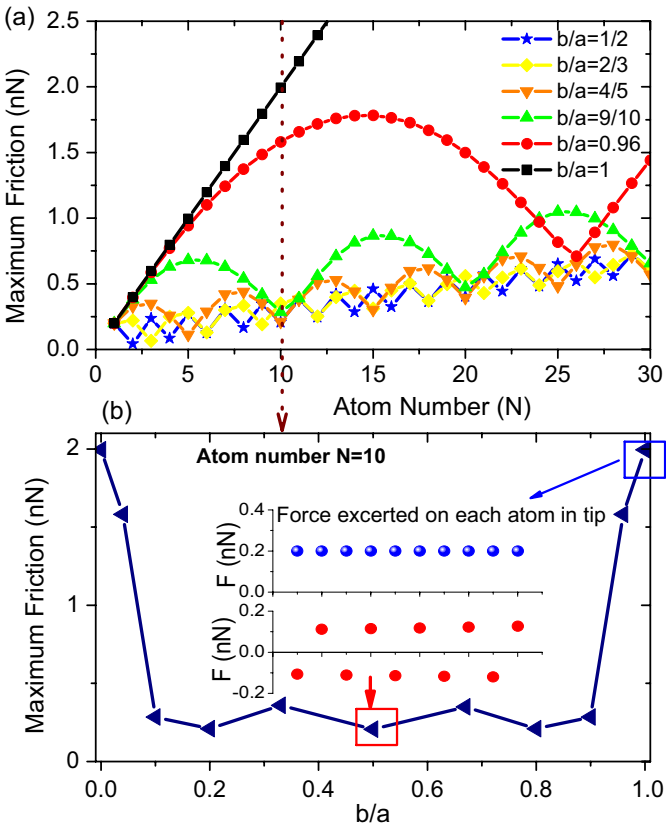

Figure 6. FKT model predictions. (*a*) Maximum friction varying with tip size, N, and the tip and substrate lattice parameters, b/a. (*b*) Variation of maximum friction with the lattice parameter ratio for the specific case of $N = 10$; the inset is the maximum friction for each of the $N = 10$ atoms.

friction as observed in figure 3. This suggests there is a quantitative connection between atomic structure and friction. While this observation cannot be extrapolated to an arbitrary contact size since another key parameter is the ratio of the Moiré pattern periodicity to the contact radius [2], for the small contact areas with which we are able to observe wear-less sliding in our simulations, the relationships identified are generally applicable.

To better illustrate the underlying mechanisms, we turn to the 1D FKT model as an analogy for the system. In the FKT model, the misalignment-induced mismatch of lattices can be mimicked by varying b/a, and the contact size can be adjusted by changing N, see figure 2. In an extreme case where the atoms are strongly coupled, $k_2 = \infty$, and there is no energy dissipation, $\mu = 0$, the friction can go to zero if $(bN/a) = n$ where n is an integer. This means there exist some specific sizes N, called magic sizes in a previous work, at which the friction is extremely small [7]. In practice, these magic sizes and friction behaviors depend on the mismatch b/a as well as the elastic coupling k_2, and if k_2 is small the friction may not be insignificant.

The predictions of the FKT model are shown in figure 6(*a*). As expected, friction varies with both b/a and tip size N. In addition, the local friction minima appear in the vicinity of $(bN/a) \simeq n$ (for example, at N=10 and $(b/a) = 9/10, n = 9$, and at $N = 15$ and $(b/a) = 4/5$, $n = 12$). A case of $N = 10$ is of particular interest because it is reflective of the size of the

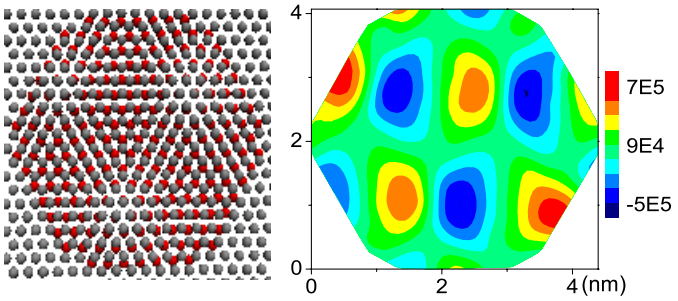

Figure 7. Moiré pattern (left) where the silver dots are substrate atoms and the red dots are tip atoms and the corresponding shear stress distribution (right) for lattice mismatch-induced incommensurability exhibited by the Ag/Cu system.

MD contact in any one direction. Figure 6(*b*) shows the variation of maximum friction with b/a for this tip size. The frictional variation can be understood by looking at the distribution of forces on the ten atoms in the contact. For example, if $(b/a) = 1$, at any given time all tip atoms will experience the same force such that the sum of their forces is large. Alternatively, if $(b/a) = 0.5$, the force varies from atom-to-atom and as a result the total maximum force is small. Another observation that can be made from figure 6(*a*) is, regardless of the tip size, the friction at $(b/a) = 1$ is much larger than that at any other lattice configuration. This is consistent with the expectation that aligned contact will yield high friction.

Although the predictions of the 1D FKT model and the fully atomistic MD model cannot be quantitatively compared, they give complementary insight into the relationship between atomic structure and friction force. For example, MD predicts for this contact size that misalignment ($\theta \neq n \times 60^\circ$) will result in an inhomogeneous shear stress distribution as shown in figure 4 and low friction as shown figure 3. The FKT model for $N = 10$ predicts similar behavior where the low friction cases observed in figure 6(*b*) at $(b/a) \neq 1$ can be correlated with the variation of force felt by the multiple atoms in the contact shown in the inset. The agreement between the MD and FKT model trends reveals that the friction variation in both systems results from the same underlying mechanism, i.e. the structural inhomogeneity.

Lastly, we investigate if the observations made in this section based on the misalignment-induced incommensurability are also applicable to lattice mismatch-induced incommensurability. We study a copper–silver interface where atomic interactions are modeled using EAM with parameters developed by Mishin *et al* [25]. The simulation setup remains the same as the Pt/Au model except the contact radius is increased to 2 nm to facilitate observation of the Moiré patterns. This system is clearly incommensurate even when the surfaces are aligned because of the difference in their lattice parameters ($a_{\mathrm{Ag}} = 0.407$ nm and $a_{\mathrm{Cu}} = 0.365$ nm). Figure 7 illustrates the Moiré pattern and shear stress distribution for this system with aligned surfaces. The non-uniform shear stress is characteristic of incommensurate contact and, as was observed with the misalignment-induced incommensurability of the Pt/Au system, is consistent with the Moiré pattern.

3.2. Slip mechanisms

In this section we investigate differences in the method by which the tip slips over the substrate in aligned and misaligned contact. To illustrate these two types of contact, we present results for the Pt/Au system with relative rotations of 0° and 10°, where the latter orientation was chosen as characteristic of misaligned angles that exhibit clear stick–slip. We start by considering

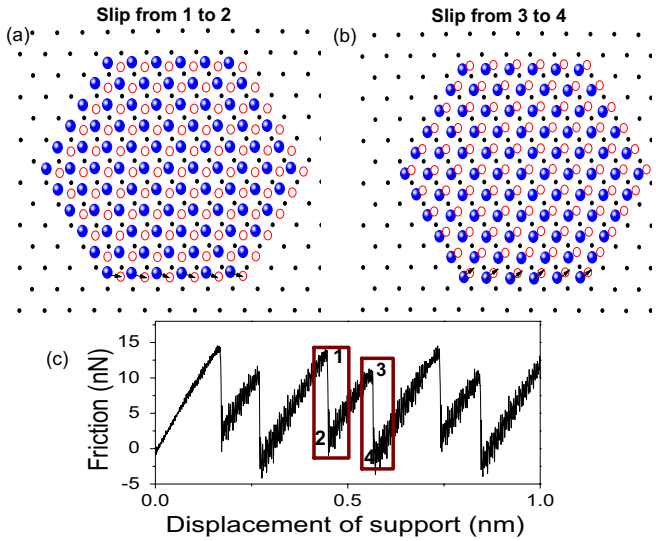

Figure 8. (*a*), (*b*) Positions of the atoms in the interface at 0° relative rotation (black dots—substrate, blue circles—tip atom starting position, red circles—tip atom ending position) before and after a slip event, and (*c*) the corresponding friction force as a function of the displacement of the tip support.

the friction traces for aligned and misaligned contacts shown in figures 8 and 9, respectively. Comparing these force traces, we observe the following similarities. First, both exhibit the saw-tooth pattern with respect to the support position (i.e. displacement of the rigid atoms at the top of the tip) that is characteristic of stick–slip motion. Second, in both cases, the periodicity of the peak friction is a multiple of the lattice spacing of the Au{1 1 1} surface ($a = 2.88$ nm). However, consistent with figure 3, the friction (both average and maximum) in aligned contact (0°) is larger than that for misaligned contact (10°). We showed in the previous section that this is due to the atomic positions and corresponding shear stress distribution. We now consider what this difference means in terms of how the system evolves during the slip process.

In aligned contact, we can see from figure 8(*c*) that the friction exhibits two distinct slip events as the support moves through a distance of $a = 0.288$ nm. Two slip events are identified on the figure as the change in friction from point 1 to 2 and from point 3 to 4. The atomic positions before and after each slip shown in figures 8(*a*) and (*b*) indicate that slip occurs via a zigzag pattern as has been reported previously [26]. To complete one period, the tip transitions from fcc (face centered cubic) to hcp (hexagonal close packed) at the first slip, and then from hcp to fcc at the second slip.

To gain a better understanding of this process, we analyze the positions of the atoms in the interface every 0.8 ps during the slip from points 1 to 2 and from 3 to 4. The corresponding distributions of atomic displacement are given in figures 10 and 11. During the transition from fcc to hcp, the atomic movement begins at the upper-left corner of the interface and then travels diagonally (relative to the sliding direction) through the contact area as shown in figure 10. A similar phenomenon occurs during the transition from hcp to fcc except that the atomic movement occurs along the other diagonal as shown in figure 11.

The friction trace for misaligned contact and the corresponding atomic positions before and after slip are shown in figure 9. It can be observed that only one slip, such as that identified from point 1 to 4, occurs during the period $a = 0.288$ nm. In addition, figure 9(*b*) shows that there is a shoulder in the friction trace during each slip (from point 2 to 3). This feature implies

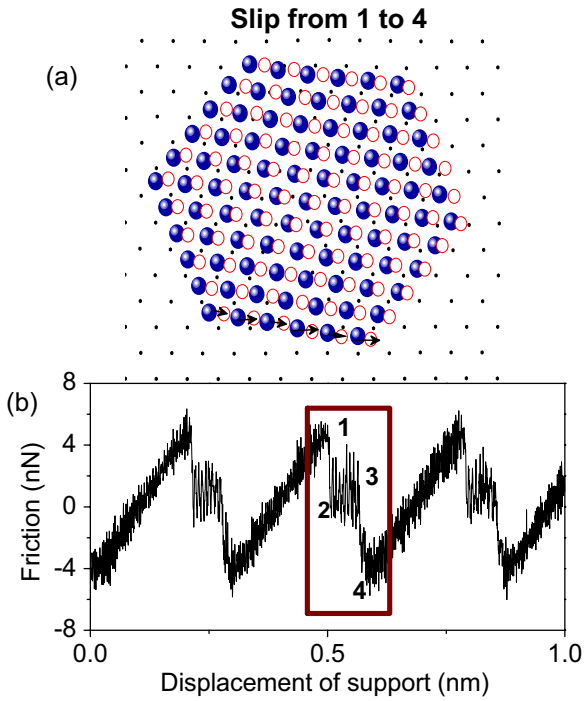

Figure 9. (*a*) Positions of the atoms in the interface at 10° (black dots—substrate, blue circles—tip atom starting position, red circles—tip atom ending position) before and after a slip event, and (*b*) corresponding friction trace.

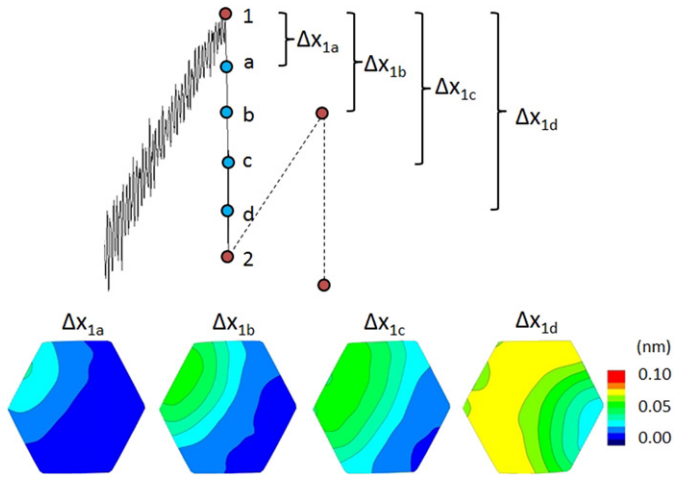

Figure 10. Change in atomic positions for commensurate contact corresponding to slip from point 1 to point 2 identified on the friction trace in figure 8. The contour plots show the *change* in position of atoms in the x-direction.

there is a metastable state at that point. To understand how the metastable state occurs, we plot the relative displacements from 1 to 2 and from 3 to 4, and the shear stress distributions at 1, 2, 3 and 4 in figure 12. It can be observed that the atoms do not move all at once. From 1 to 2, a subset of the atoms slip forward and a metastable state is formed. Then, with the increasing

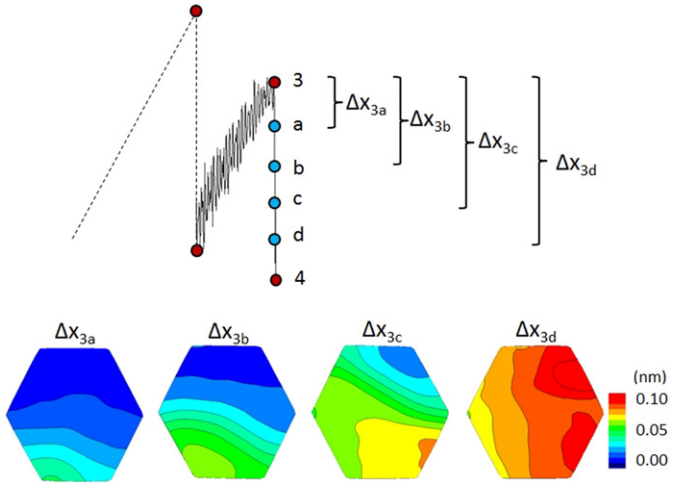

Figure 11. Change in atomic positions for commensurate contact corresponding to slip from point 3 to point 4 identified on the friction trace in figure 8. The contour plots show the *change* in position of atoms in the x-direction.

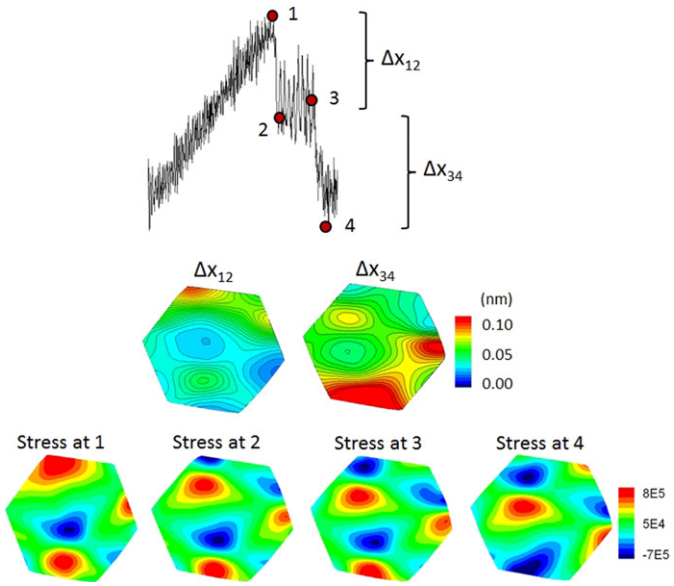

Figure 12. Change in atomic positions during the slip for incommensurate contact corresponding to the friction trace in figure 9. The contour plots show the *change* in position of the atoms in the x-direction from point 1 to 2 and then from 3 to 4, and the shear stress distributions at points 1, 2, 3 and 4.

external push from the support, the metastable state breaks down and the remaining atoms slip forward resulting in the transition from position 3 to 4. The discontinuity in this process is also visible in the shear stress distributions.

One effect of the metastable state is an increase in the duration of a slip event. For example, the duration of slip from 1 to 4 in the misaligned case shown in figure 9 is 22 times longer than the duration of slip from 1 to 2 in the commensurate case shown in figure 8. Prolonged slip has

been observed experimentally and has been suggested to be a result of multiple contacts [27]. The existence of prolonged slip in our simulations, where there is explicitly only one contact, suggests that metastable states may also contribute to increased duration of some slip events.

The slip mechanisms revealed in figures 10, 11 and 12 also give some insight into the role of multi-stability in atomic friction. It has been suggested that friction at the atomic scale depends on the competition between elastic restoring forces in the bulk of the tip and interfacial interactions [5, 28]. Metastable states that exist 'internally' at the interface can lead to local pinning and additional energy dissipation [29]. In our simulations with aligned interfaces, the stick–slip instability is associated with the tip moving as a whole via a single dislocation sweeping across the interface. In contrast, for the simulations with misaligned interfaces, there exist internal meta-stable states, and the instabilities are associated with inhomogeneous slips in the interface.

Finally, visual analysis of the displacement and stress distributions for misaligned contact in figure 12 reveals that the atomic displacement pattern is qualitatively consistent with that of the shear stress. Inhomogeneous (sometimes called unbalanced) shear stresses can be relieved by the formation of dislocations which then propagate during relative sliding [26, 30, 23]. Therefore, our results suggest that, like the sliding of aligned surfaces, misaligned surface sliding occurs via dislocation propagation, albeit a more complicated one as revealed by the detailed patterning of the shear stress. These results provide qualitative support for the hypothesis that, in aligned contact, relative motion is resisted by regularly spaced dislocations, whereas in misaligned contact, motion is resisted only by 'disassociated aperiodically spaced' dislocations and the overall friction is small [31].

4. Conclusion

The goal of this study was to understand the connection between friction and atomic structure in the buried interface. To make this connection, we used a fully atomistic model with interatomic potentials partially validated by first principles calculations to predict friction and shear stress and also atomic positions before, during and after slip in aligned and misaligned contact. Quantitative links were made between atomic superstructures and the interface shear stress distributions, and these relationships were studied further using the 1D FKT model. We also investigated the effect of atomic structure on the way surfaces move relative to one another and found evidence for dislocation-mediated slip in both aligned and misaligned contacts. It is relevant to note that all the observations reported in this paper were made using clean crystalline surfaces whereas under experimental conditions, especially AFM measurements taken in air, there may be debris or third bodies which result in large friction forces in systems that would otherwise be expected to be incommensurate [9]. Atomic friction may also be affected by surface roughness [19]. However, under the idealized conditions that many experiments are now striving for, for example in a controlled ultra-high vacuum environment with an atomically flat substrate, the simulations results presented here are highly relevant. More importantly, the connection between structure, contact shear stress, atomic dislocation and friction is fundamental and illustrates the critical role of buried interface in understanding atomic-scale friction.

Appendix A: Pt–Au interaction model

All atomic interactions are described by the embedded atom model (EAM). The Cu–Cu, Ag–Ag and Cu–Ag interactions are modeled using parameters developed by Mishin *et al*

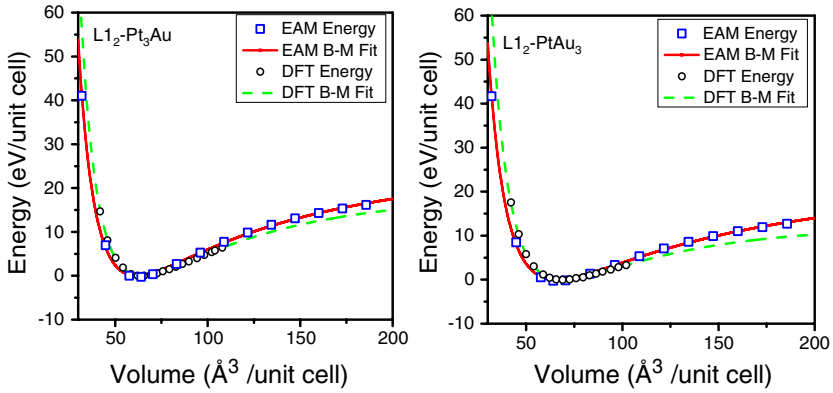

Figure 13. Comparison of DFT and EAM-calculated energies and their fitted Birch–Murnaghan equations of state as a function of lattice volume for structures $L1_2$-Pt_3Au and $L1_2$-$PtAu_3$.

[25]. Parameters developed by Voter and Chen [32] are used to describe Au–Au and Pt–Pt interactions. However, to the best of the authors' knowledge, a validated model for Au–Pt interactions is not available. Therefore, as a first approximation, the interaction between Au and Pt atoms is calculated by the arithmetic mean of the pure material pair potentials. The EAM electron density function for Au is then re-scaled to identify a single summed electron density that matches Pt. Density functional theory (DFT)-based *ab initio* calculations are performed as a benchmark to evaluate this cross-pair potential.

All DFT calculations are performed using the WIEN2k [33] software, in which the full-potential linearized augmented plane-wave method [34] is used to solve the Kohn–Sham equations. The exchange-correlation energy function is described with the Perdew–Burke–Ernzerhof-96 generalized gradient approximation [35]. Core states are treated fully relativistically while for valence states relativistic effects can be included either in a scalar relativistic treatment or with the second variational method including spin-orbit coupling. For all calculations, the radii of muffin-tin spheres for both Pt and Au are 2.4 bohr, and the energy to separate core states and valence states is -6.0 Ry. $RKMAX$ and $l_{\max}$, parameters that determine the number of basis and radial functions, are set to 8 and 10, respectively. The calculations are iterated until the total energies are converged to less than 0.0001 Ry.

Calculations are performed for six hypothetical metallic compounds, B2-PtAu, B1-PtAu, $L1_2$-Pt_3Au, $L1_2$-$PtAu_3$,$D0_9$-$PtAu_3$ and $D0_9$-Pt_3Au, where the indexing corresponds to the Strukturbericht designation. The total energies are calculated as a function of volume and fitted to the third-order Birch–Murnaghan isothermal equation of state [36] to obtain the ground state bulk properties. The equation of states calculated using DFT and EAM for two representative compounds are shown in figure 13. Since the DFT-calculated energies are relative to a zero-point that is defined arbitrarily, we set the energies for both DFT and EAM at the equilibrium state to zero in the figure. Table 1 shows the fitted lattice constants, bulk moduli and their pressure derivative for the six metallic compounds. The equation of states and bulk properties calculated using DFT and EAM agree well with each other, though some deviations are observed. It should be noted that the lattice spacing predicted by DFT using the Perdew–Burke–Ernzerhof functional is expected to be an overestimate of experimental measurements (for the pure materials, we find the overestimate to be 1.05% for Pt [37] and 1.84% for Au [38]). Therefore, the small amount by which the EAM lattice constants are larger than those predicted by DFT may in fact indicate better accuracy.

Table 1. Lattice constant (a_0), bulk modulus (B_0) and pressure derivative of bulk modulus at equilibrium volume (BP) calculated with DFT in comparison with EAM calculations.

	a_0 (nm)		B_0 (GPa)		BP	
Alloy	DFT	EAM	DFT	EAM	DFT	EAM
$L1_2$-$PtAu_3$	0.410 10	0.403 81	168.9266	168.5993	6.0235	5.3148
$L1_2$-Pt_3Au	0.401 08	0.394 90	226.9575	227.2135	5.8072	5.4607
B1-PtAu	0.536 11	0.523 80	142.9471	170.3370	5.6160	5.4270
B2-PtAu	0.322 36	0.317 35	226.0533	222.7419	5.8134	5.7481
$D0_9$-$PtAu_3$	0.514 02	0.493 79	51.7994	64.4412	5.6468	5.4072
$D0_9$-Pt_3Au	0.501 94	0.482 80	67.7842	80.1361	5.6606	5.4772

In summary, the results show that the simple, arithmetic mean Pt–Au cross-pair potential is able to successfully generate six intermetallic compounds which is a demonstration of its accuracy. A more accurate cross potential for Pt–Au, particularly to capture the surface behavior, requires a more complicated fitting procedure, and corresponding research is currently underway.

Acknowledgments

The authors are grateful for insightful discussions with Drs Laurence Marks, Robert Carpick and Danny Perez, as well as to the National Science Foundation for its support via awards CMMI-0758604 and CMMI-0800154.

References

[1] Holscher H, Schirmeisen A and Schwarz U D 2008 Principles of atomic friction: from sticking atoms to superlubric sliding *Phil. Trans. R. Soc.* A **366** 1383–404
[2] Hirano M, Shinjo K, Kaneko E and Murata Y 1991 Anisotropy of frictional forces in muscovite mica *Phys. Rev. Lett.* **67** 2642–5
[3] Crossley A, Kisi E H, Summers J W B and Myhra S 1999 Ultra-low friction for a layered carbide-derived ceramic, Ti_3SiC_2, investigated by lateral force microscopy (LFM) *J. Phys. D: Appl. Phys.* **32** 632
[4] Dienwiebel M, Verhoeven G S, Pradeep N, Frenken J W M, Heimberg J A and Zandbergen H W 2004 Superlubricity of graphite *Phys. Rev. Lett.* **92** 126101
[5] Müser M H 2004 Structural lubricity: role of dimension and symmetry *Europhys. Lett.* **66** 97–103
[6] Weiss M and Elmer F J 1996 Dry friction in the Frenkel–Kontorova–Tomlinson model: static properties *Phys. Rev.* B **53** 7539–49
[7] Igarashi M, Natori A and Nakamura J 2008 Size effects in friction of multiatomic sliding contacts *Phys. Rev.* B **78** 165427
[8] Kim W K and Falk M L 2009 Atomic-scale simulations on the sliding of incommensurate surfaces: the breakdown of superlubricity *Phys. Rev.* B **80** 235428
[9] He G, Müser M H and Robbins M O 1999 Adsorbed layers and the origin of static friction *Science* **284** 1650
[10] Müser M H and Robbins M O 2000 Conditions for static friction between flat crystalline surfaces *Phys. Rev.* B **61** 2335–42
[11] Li Q, Dong Y, Perez D, Martini A and Carpick R W 2011 Speed dependence of atomic stick–slip friction in optimally matched experiments and molecular dynamics simulations *Phys. Rev. Lett.* **106** 126101
[12] Gosvami N N, Filleter T, Egberts P and Bennewitz R 2010 Microscopic friction studies on metal surfaces *Tribol. Lett.* **39** 19–24
[13] Plimpton S J 1995 Fast parallel algorithms for short-range molecular dynamics *J. Comput. Phys.* **117** 1
[14] Braun O M and Kivshar Y S 2004 *The Frenkel–Kontorova Model: Concepts, Methods, and Applications* (Berlin: Springer)
[15] Riedo E, Gnecco E, Bennewitz R, Meyer E and Brune H 2003 Interaction potential and hopping dynamics governing sliding friction *Phys. Rev. Lett.* **91** 084502

[16] Ashby M, Shercliff H and Cebon D 2009 *Materials: Engineering, Science, Processing and Design* (Oxford, UK: Butterworth-Heinemann)
[17] Reimann P and Evstigneev M 2005 Description of atomic friction as forced Brownian motion *New J. Phys.* **7** 25
[18] Bennewitz R, Gyalog T, Gussisberg M, Bammerlin M, Meyer E and Guntherodt H J 1999 Atomic-scale stick–slip processes on Cu(1 1 1) *Phys. Rev.* B **60** R11301–R11304
[19] Qi Y, Cheng Y, Çağin T and Goddard W A III 2002 Friction anisotropy at Ni (1 0 0)/(1 0 0) interfaces: molecular dynamics studies *Phys. Rev.* B **66** 085420
[20] Filippov A E, Dienwiebel M, Frenken J W M, Klafter J and Urbakh M 2008 Torque and twist against superlubricity *Phys. Rev. Lett.* **100** 046102
[21] Bonelli F, Manini N, Cadelano E and Colombo L 2009 Atomistic simulations of the sliding friction of graphene flakes *Eur. Phys. J.* B **70** 449–59
[22] Zhou M 2003 A new look at the atomic level virial stress: on continuum-molecular system equivalence *Pro. R. Soc. Lond.* A **459** 2347–92
[23] Merkle A P and Marks L D 2007 a predictive analytical friction model from basic theories if interfaces, contacts and dislocations *Tribol. Lett.* **26** 73
[24] Lopes dos Santos J M B, Peres N M and Neto A H C 2007 Graphene bilayer with a twist: electronic structure *Phys. Rev. Lett.* **99** 256802
[25] Williams P L, Mishin Y and Hamilton J C 2006 An embedded-atom potential for the Cu–Ag system *Model. Simul. Mater. Sci. Eng.* **14** 817
[26] Sørensen M R, Jacobsen K W and Stoltze P 1996 Simulations of atomic-scale sliding friction *Phys. Rev.* B **53** 2101–13
[27] Maier S, Sang Y, Filleter T, Grant M, Bennewitz R, Gnecco E and Meyer E 2005 Fluctuations and jump dynamics in atomic friction experiments *Phys. Rev.* B **72** 245418
[28] Müser M H, Urbakh M and Robbins M O 2003 Statistical mechanics of static and low-velocity kinetic friction *Adv. Chem. Phys.* **126** 187–272
[29] Prandtl L 1928 A conceptual model to the kinetic theory of solid bodies *Z. Angew. Math. Mech.* **8** 85–106
[30] Hurtado J A and Kim K S 1999 Scale effects in friction of single-asperity contacts: I. From concurrent slip to single-dislocation-assisted slip *Pro. Roy. Soc. Lond.* A **455** 3363–84
[31] Merkle A P and Marks L D 2007 Comment on friction between incommensurate crystals *Phil. Mag.* **87** 527–32
[32] Voter A F 1993 Embedded atom method potentials for seven fcc metals: Ni, Pd, Pt, Cu, Ag, Au and Al *Los Alamos Unclassifed Technical Report LA-UR-93-3901*
[33] Schwarz K and Blaha P 2003 Solid state calculations using wien2k *Comput. Mater. Sci.* **28** 259–73
[34] Singh D 1994 *Plane Waves, Pseudopotentials and the LAPW Method* (Dordrecht: Kluwer)
[35] Perdew J P, Burke K, and Ernzerhof M 1996 Generalized gradient approximation made simple *Phys. Rev. Lett.* **77** 3865–68
[36] Birch F 1947 Finite elastic strain of cubic crystals *Phys. Rev.* **71** 809–24
[37] Da Silva J L F, Stampfl C, and Scheffler M 2006 Converged properties of clean metal surfaces by all-electron first-principles calculations *Surf. Sci.* **600** 703–15
[38] Leung K, Rempe S B, Schultz P A, Sproviero E M, Batista V S, Chandross M E and Medforth C J 2006 Density functional theory and DFT + U study of transition metal porphines adsorbed on Au(1 1 1) surfaces and effects of applied electric fields *J. Am. Chem. Soc.* **128** 3659–68